

Epitaxial Growth of Ruthenium Dioxides on Ru(0001) Surface

C.-H. Nien and M.S. Zei*

Department of Physics, National Central University, No.300 Jungda Rd., Jungli 32001, Taiwan

*Correspondence to:

Dr. M.S. Zei

Department of Physics, National Central University, No.300 Jungda Rd., Jungli 32001 Taiwan

E-mail: zei@phy.ncu.edu.tw

Received: August 23, 2016

Accepted: November 07, 2016

Published: November 11, 2016

Citation: Nien CH, Zei MS. 2016. Epitaxial Growth of Ruthenium Dioxides on Ru(0001) Surface. *NanoWorld J* 2(3): 52-62.

Copyright: © 2016 Nien and Zei. This is an Open Access article distributed under the terms of the Creative Commons Attribution 4.0 International License (CC-BY) (<http://creativecommons.org/licenses/by/4.0/>) which permits commercial use, including reproduction, adaptation, and distribution of the article provided the original author and source are credited.

Published by United Scientific Group

Abstract

The epitaxial growth of the RuO₂ clusters on Ru(0001) electrode formed by electrooxidation in HClO₄ solution has been studied by ex-situ reflection high energy electron diffraction (RHEED), low energy electron diffraction (LEED) and Auger electron spectroscopy (AES) after emersion. The LEED pattern for the RuO₂ clusters on Ru(0001) exhibits a (1 x 1) phase, while both Ru-oxide and substrate reflections are observed by RHEED, so that the crystal structure of RuO₂ clusters has been determined by RHEED rather than LEED. Sample annealing at 700 K° for 11 min sharpens the RHEED reflections facilitating the determination of the structure of RuO₂ clusters. That is, the RuO₂ clusters are exclusively (100) oriented, monocrystalline despite the crystal disorder, and three (100) RuO₂ domains rotated by 120° with each other grown on Ru(0001). Furthermore, it is found that the crystallinity of RuO₂ grains formed at +1.98 V is even worse than that at +1.12 V. Under oxidation conditions the hydroxyl OH⁻ anions are chemisorbed on Ru(0001) electrode inducing the segregation of Ru-atoms to surface. The Ru-atoms turn to react with the OH_{ad}⁻ species to bulk hydroxide RuOH, causing surface roughening and formation of three dimensional (3D) RuO₂ cluster via a Vollmer-Weber growth mode on Ru(0001).

Keywords

Reflection high-energy electron diffraction (RHEED), Low energy electron diffraction (LEED), RuO₂ cluster

Introduction

RuO₂ in both crystalline and amorphous phases features special properties, such as metallic conductivity and catalytic activities [1-2]. The promising applications of RuO₂ range from electronic advancement in integrated circuit, film resistors, ferroelectric films to high-temperature superconducting thin films in forming a buffer layer [3-5]. The oxygen evolution reaction (OER) occurs at a suitable reaction rate on noble metals (e.g., Pt, Au, Ir, Ru and Ag), while metal oxides (RuO₂ and IrO₂) are generally more active electrocatalysts for this reaction than metal electrodes [6-8]. RuO₂ as active and stable anodes can be used for chlorine generation in the chlor-alkali industry, oxygen or hydrogen evolution in water electrolysis [9, 10], CO₂ reduction in photocatalysis, and CO oxidation in sensors [1, 11, 12]. The activity and selectivity of Ru oxides depend largely on the oxidation state of the metal, and the essential surface reaction of the RuO₂ electrode is expected to cover the full range of Ru²⁺, Ru³⁺, and Ru⁴⁺ oxidation states [13]. Recently, oxygen-rich Ru(0001) surfaces have been shown to be very active for the conversion of CO to CO₂, even under UHV conditions where the pure or adsorbed-oxygen-covered Ru(0001) surfaces are virtually inactive [14, 15]. The

Ru(0001) surface was oxidized to RuO_2 by exposure to large amounts of molecular oxygen at elevated sample temperatures (600-800 K) under UHV conditions, growing epitaxially with (110) face on Ru(0001) [16], while single crystals of (100) RuO_2 are grown in a multizone furnace using a vapor transport method under oxygen flow [12]. On the other hand, the ruthenium oxide films were electrodeposited on tin doped indium oxide (TIO) substrate from an aqueous solution, for which the monocrystalline phase was characterized by XRD measurements [17], while the hydrous $\text{RuO}_2 \cdot n\text{H}_2\text{O}$ prepared by voltammetric deposition on titanium electrode exhibited an amorphous phase [18]. Electrodeposition is a powerful and interesting process that can be applied in numerous fields. In addition to a low process temperature, low cost in equipment and a negligible waste of material, electrode position also exceeds other techniques by the ability to deposit films on a complex surface. In the present work the ruthenium dioxide has been prepared by electrochemical oxidation on Ru(0001) electrode in HClO_4 electrolyte solution. So far, little work has been reported for RuO_2 prepared by electrooxidation of single crystal Ru, and there have been no studies of epitaxial growth of single crystal (100) RuO_2 on Ru(0001). It is the aim of this paper to show that LEED pattern exhibits only a (1 x 1) phase, while both Ru-oxide and the Ru substrate reflections are observed by RHEED for the Ru(0001) electrode toward electrooxidation in 0.01 M HClO_4 , proving the extra spots are consisted of different zone-axis patterns of RuO_2 domains on Ru(0001). Analysis of the RHEED patterns offers an effective way to determine the epitaxial growth of RuO_2 and lateral orientations of the (100) RuO_2 domains on Ru(0001).

Structural determination of the deposits on electrode surfaces by LEED and RHEED

Determination of the adlayer structures on substrate surface by LEED/RHEED:

The two dimensional (2D)-reciprocal lattice (RL) is expressed by the equation, $\vec{u}_{hk} = H\vec{b}_{10} + K\vec{b}_{01}$, where H, K are the integer numbers, and $\vec{b}_{10}, \vec{b}_{01}$ the RL unit cell vectors of adlayer on substrate. In the following H, K and L are normalized to the substrate lattice parameters. By letting H or K to be non-zero, one may probe the atomic coordinates along the surface plane, e.g., determining the adlayer structure with respect to the substrate surface. The reciprocal lattice parameters, $|\vec{u}_{hk}| = r \cdot \frac{1/\lambda}{L_1}$ are determined from the RHEED patterns, where $|\vec{u}_{hk}|$ is the magnitude of an RL vector, L_1 is the camera length (the distance between the sample and the screen), r is the reflection rod-spacing or spot-spacing in millimeter calibrated from the millimeter scale adhered on the screen (refer to Figure 1), and λ is the wavelength of the RHEED electron beam [19-21]. The millimeter scale adhered on the screen is used to measure the RL-distances of the reflections in RHEED when the substrate signal is completely blocked by the deposit. For instance, the lengths of the unit cell vectors \vec{b}_{10} and \vec{b}_{01} of an fcc (111) plane are determined from the reflection rod-spacing of the [110] and [211] azimuths RHEED patterns, respectively that are the reciprocal values of the [110] and [211] atomic row spacings of the (111) substrate, where the $[uvw]$ atomic

rows are parallel to the electron incident direction (azimuth). The hexagonal Ru(0001) surface has a $(a_1 \times a_2)$ unit cell with $a_1 = a_2 = 2.71 \text{ \AA}$, and the lengths of \vec{b}_{10} is the reciprocal value of the $[10\bar{1}0]$ atomic row spacing, that is $\vec{b}_{10} \perp \vec{a}_2$ while $\vec{b}_{01} \perp \vec{a}_1$. The $[uvw]$ zone-axis pattern (ZAP) of a 3D lattice is a diffraction pattern taken with an incident beam e.g., of electrons, X-rays traveling along a lattice direction specified by the zone-axis indices $[uvw]$. Because of their small wavelength λ , the high energy electrons (30- 40 keV) have a very large Ewald sphere radius ($1/\lambda$) so that electron diffraction generally "lights up" diffraction spots with g -vectors (hkl) that are perpendicular to $[uvw]$. In other words, the intersection of a three dimensional (3D) reciprocal lattice by the reflection sphere results in a reciprocal lattice plane, in which the intercept points (HKL) are the RL points (relps) fulfilled under the zone condition, $Hu + Kv + Lw = 0$. The LEED/RHEED patterns are the cross section of an RL projected onto the LEED/RHEED screens, e.g., the LEED pattern exhibits the superimposed diffraction spots of different Ru-oxide domains, which allows the determination of lateral orientations of the oxide-domains grown on substrate surface. The same holds for RHEED. The crystalline phase of deposit is accordingly determined by the acquired reciprocal lattice by LEED/RHEED [22, 23].

The number of the adlayers is estimated by the interference function as following;

$$F(s) = \frac{\sin^2 \pi N_3 s \bar{c}}{\sin^2 \pi s \bar{c}}$$
, where N_3 is the number of layers, s and c are the RL- and the lattice-vector perpendicular to the surface, respectively [24].

The experimental set-up for characterization of adlayer on electrode surfaces by ex-situ LEED/RHEED and AES is shown in Figure 1. The LEED electrons with wave vector k_0 impacts perpendicularly to the sample surface, the elastically diffracted electrons with wave vector k are accelerated by the grid potential of +3.8 keV and crush the fluorescent screen lighting up the reflection spots. On the other hand, the RHEED experiment was performed with an electron beam energy of 40 keV (with a wave vector k_0) at grazing incidence of 2-3° and the elastically diffracted electrons give

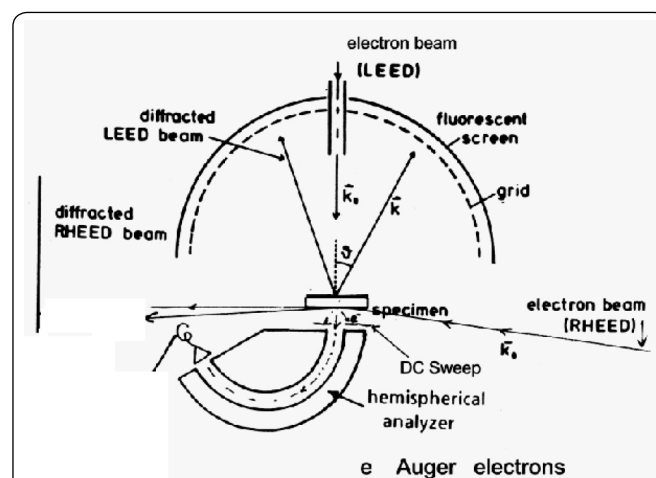
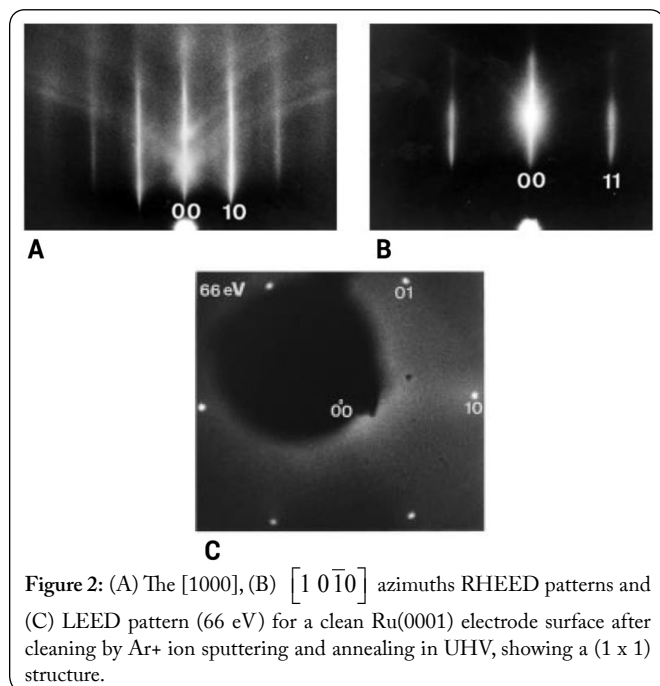


Figure 1: Experimental set-up for surface studies by LEED, RHEED and AES. The wave vectors k_0, k are the incoming and diffracted electron beams, respectively which are impacted on and scattered from the sample surfaces.

the RHEED patterns, while the released Auger electrons are discriminated via a hemispherical analyzer, resulting in an Auger electron spectrum (AES). This experimental set-up allows the correlation between the surface structure and the chemical composition on the electrode surfaces [25].

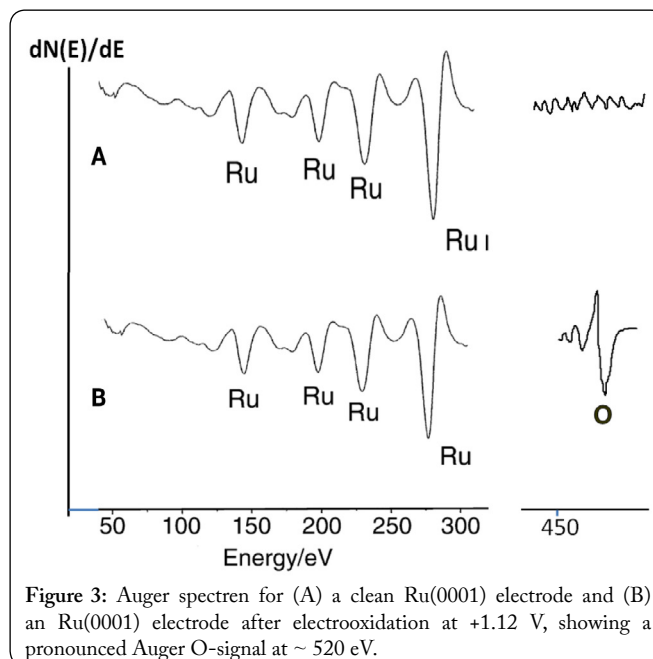
Preparation of a clean electrode surface

For the sake of convenience, we will briefly recall the preparation procedures of clean electrode surfaces which have been previously reported [19]. A clean Ru(0001) electrode surface was prepared by cycles of sputtering and annealing in an UHV chamber until a well-ordered and clean surface emerges, which can be monitored by LEED/RHEED and AES as seen in Figures 2A, B, C and 3A, respectively. The typical conditions used for Ru single crystal surface are conducted by argon ion sputtering (with 500-800 eV) for ca. 45 min at 5×10^{-5} torr and annealing by resistive heating at ≈ 700 °C for 20-30 min. The (1×1) LEED/RHEED patterns in Figure 2 show sharp reflection spots/streaks for a clean Ru(0001) surface, exhibiting a well-ordered Ru(0001) surface. The Auger spectrum in Figure 3A shows no impurities signal for the prepared Ru surface, e.g., O-Auger signal. The samples were moved between UHV chamber and the electrochemical cell via a closed-transfer system [19]. The chemisorption of metal/anion onto electrode surfaces was conducted in the electrochemical cell, and the detailed procedures have been described elsewhere [20]. The experimental set-up for characterization of electrode surfaces by ex-situ LEED/RHEED and AES is shown by Figure 1. This experimental set-up allows the characterization of the surface structure and the chemical composition on electrode surfaces.



Electrochemical experiments

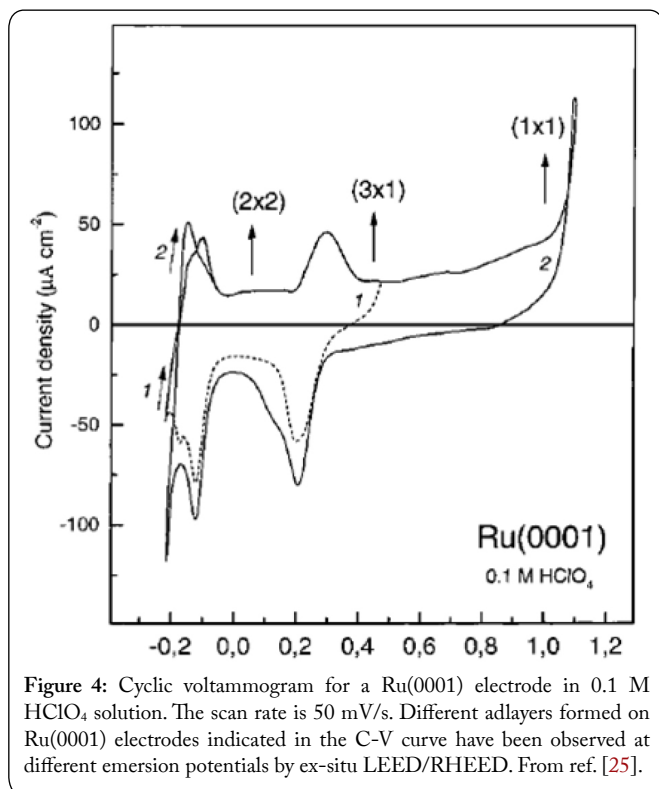
Prior to electrochemical experiments the cleanliness and crystal ordering of the UHV-prepared Ru(0001) electrode were firstly examined by both LEED/RHEED (see Figure 2) and AES measurements (Figure 3A). Then Ru(0001) electrode



was transferred to the electrochemical chamber, which was floated with 5.0 N argon gas afterward. The 5.0 N nitrogen overpressure was efficient to keep air out of the electrochemical cell at all stages of the experiments. A glass capillary, filled with an aqueous electrolyte of 0.1 M HClO₄, was moved to pass through a gate valve from its lower position into the electrochemical chamber. The Ru(0001) electrode surface was then allowed to contact the solution via a meniscus configuration under potential control. The electrolyte was prepared by Millipore water (>18 M Ω) and suprapure-grade perchloric acid HClO₄ (Merck). All experiments were performed at room temperature, and all potentials are given versus the Ag/AgCl electrode in saturated KCl solution. The UHV-prepared Ru(0001) electrode was subjected to potential cycling in the HClO₄ solution in a defined potential range and the electrochemical data were recorded as illustrated in Figure 4. After the electrochemical experiments are completed, the electrode was tilted close to vertical position in order to facilitate solution draining to the edge of the surface, where the drop was stripped off via a thin Teflon tubing attached to a syringe (dry emersion). At last, the electrochemical cell was withdrawn to its original lower position. After the gate valve was closed, the argon gas was first removed by a sorption pump (with liquid nitrogen) for 2 min, followed by evacuating the electrochemical chamber to 10^{-7} mbar before the sample was quickly transferred back into the main UHV chamber. After emersion the adlayer structure on Ru electrode could subsequently be characterized ex situ by LEED/RHEED and AES techniques [25]. The (2×2) (3×1) and (1×1) structures have been observed at 0.1, 0.4 and 0.7 V emersion potentials, respectively referred to Figure 4 [25].

Results and Discussion

The structures of adlayer and the "as-prepared" RuO₂ clusters grown on the Ru(0001) electrode have been investigated by ex-situ LEED/RHEED after emersion. The cyclic voltammograms for a clean Ru(0001) electrode shown



in Figure 4 was conducted in a 0.1 M HClO₄ electrolyte solution [25]. Different O-adlayers are observed at different emersion potentials as indicated in Figure 4; the (2 x 2) and (3 x 1) have been observed at 0.1 and 0.4 V emersion potentials, respectively (from ref. 25), while the RuO₂ clusters grown on Ru(0001) electrode has been obtained by electrooxidation at +1.12 V for 2 min in 0.1 M HClO₄ electrolyte solution. The electrooxidation on Ru(0001) was accompanied by a pronounced anodic peak in the cyclic voltammetry as well as an increase in an O-Auger signal in AES spectrum as shown in Figure 4 and 3B, respectively [25]. The corresponding LEED pattern shows a (1 x 1) phase in Figure 5A, where only the integral-order spots appear and they become significantly broader than that of a clean Ru surface (compared to Figure 3C), proving the crystal ordering of Ru electrode is disturbed by electro-oxidation. Contrary to a (1 x 1) LEED pattern, additional spots of the Ru-oxides are observed besides the Ru substrate reflections by RHEED (Figure 5B) for the same sample surface. It is demonstrated that RHEED is substantially more sensitive than LEED for detection of nano clusters (Ru-oxide clusters) grown on Ru(0001) electrode [23, 25]. Annealing the same surface in UHV at 800 K° for 5 min leads to sharpening the reflection spots of RHEED patterns as seen in Figure 5C, suggesting that sample annealing sets in Ostwald-ripening process, i.e., increasing the nanocrystallite-sizes and crystal ordering of Ru-oxide clusters on Ru(0001). The cycles-pattern (Debye-Rings) characteristic for multi-crystalline RuO₂ was not observed by RHEED (Figure 5C), proving the Ru-oxide clusters are monocrystalline on Ru(0001). This is contrary to the previously reported works [18] which shows an amorphous phase. That extra spots in the RHEED pattern (Figure 5C and 5C) are attributed to RuO₂ clusters as explored below; prior to determining the reciprocal lattice of the RuO₂ clusters by means of RHEED, the RL

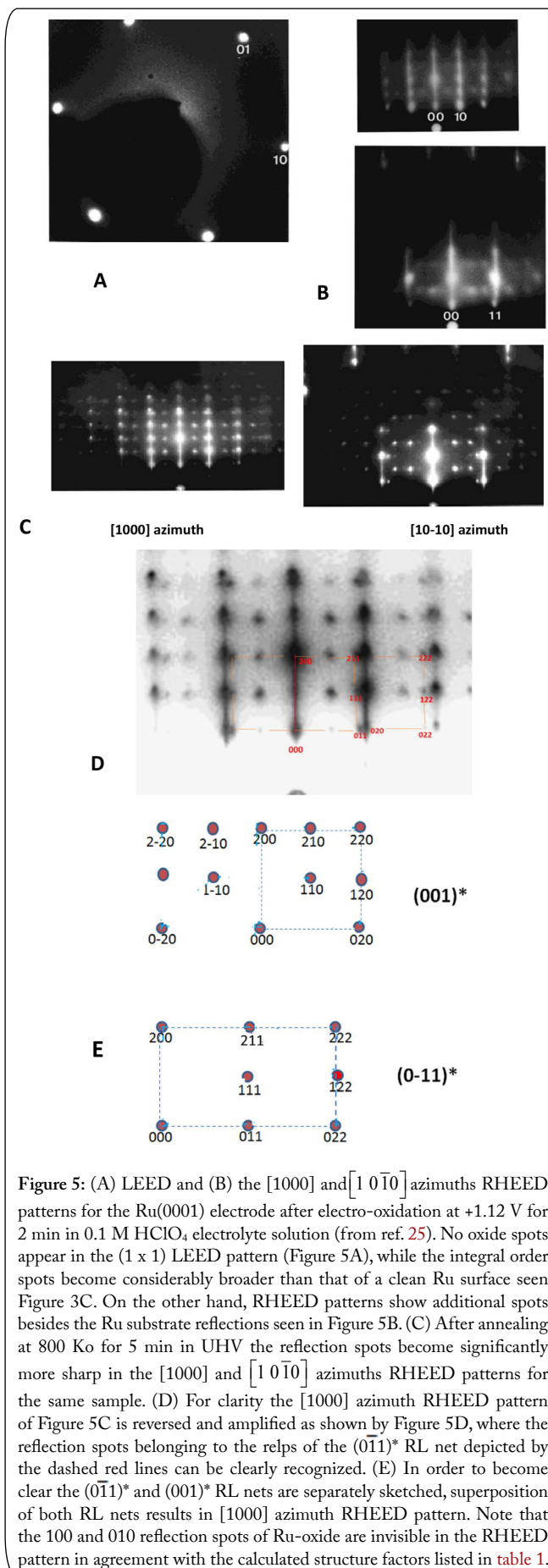


Table 1: Kinematic structure factors of RuO₂ with *b* and *k* in the *a** direction and *l* in the *c** direction.

<i>b</i>	<i>k</i>	<i>l</i>	Length (Å ⁻¹)	Structure factor
1	0	0	0.222	0
0	1	0	0.222	0
0	1	1	0.391	3655
1	1	0	0.314	5799
1	1	1	0.450	305
2	1	1	0.592	3469
2	1	0	0.497	121
2	0	0	0.445	2411
3	1	0	0.703	2021
0	0	1	0.322	0
0	0	2	0.644	4307
1	0	1	0.391	3655
0	1	2	0.681	0
1	0	2	0.681	0
2	0	0	0.445	2411
2	0	2	0.782	1330
3	0	1	0.740	3200

Several structure factors are quite small because of the centrosymmetry of the Ru sublattice and the fact that Ru is a much stronger scatterer than O. From reference [26].

parameters of a clean Ru(0001) substrate have been first determined from their RHEED patterns. The magnitudes of the unit cell vectors of b_{10} and b_{11} of the Ru(0001) substrate are 0.426 (b_{10}) and 0.738 Å⁻¹ (b_{11}) respectively that are determined from the reflection rod-spacing of the [1000] and [1 0 $\bar{1}$ 0] azimuths RHEED patterns, respectively corresponding to the reciprocal values of the [1000] and [1 0 $\bar{1}$ 0] atomic row spacing of the Ru(0001) surface. The (0001) atomic layer spacing of Ru(0001) is estimated by (0002) spot spacing of 0.467 Å⁻¹ along the Ru (11) reflection rod which gives $c = 4.28$ Å corresponding to the (0001) atomic layer spacing of bulk Ru. Referring to the RL parameters of the Ru substrate the lengths of the extra spots in the RHEED patterns (Figure 5C) are evaluated to determine the reciprocal lattice of RuO₂. For the sake of clarity, the images of the [1 0 $\bar{1}$ 0] azimuth RHEED patterns obtained at different oxidation potentials (+1.12 and 1.98 V) are reversed as shown in Figure 6A and 6B, which assists the identification of the extra spots of RuO₂ in the RHEED patterns obtained at different oxidation potentials. In a more elaborate analysis, the 101, 202, 301, 002 and 200 reflection spots of the [1 0 $\bar{1}$ 0] azimuth RHEED pattern in Figure 5C are attributed to the relps of the (010)* RL net of RuO₂ clusters as shown by the dashed blue line in Figure 7A corresponding to a [010] zone-axis pattern of RuO₂. The RL lengths of these spots in the RHEED patterns (Figure 6 and 7) are examined and in good agreement with that of hkl-spots of ruthenium dioxide listed in Table 1 [26], where the

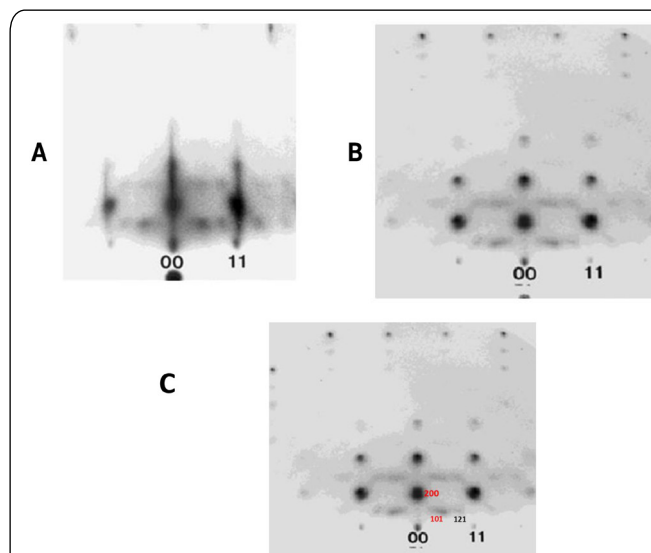


Figure 6: For better classification of the crystallinity of RuO₂ clusters grown on Ru(0001) obtained at different potentials, the images of the [1 0 $\bar{1}$ 0] azimuth RHEED patterns obtained at emersion potentials of +1.12 and +1.98 V are reversed and shown in (A) and (B), respectively. The 3D-spots of RuO₂ are observed besides the Ru-reflection streaks (11, -1-1) in the RHEED patterns in Figure (A). While the RHEED pattern (B) for the Ru(0001) electrode after electro-oxidation at +1.98 V for 21 min in 0.1 M HClO₄ electrolyte solution shows only bulk Ru spots, and the streaky Ru reflections are no longer visible in the RHEED pattern, proving the whole Ru electrode becomes rough. (B) It is demonstrated that the second order of 101 reflection spot and 002 spots of the RuO₂ produced at +1.98V are no longer visible in the [1 0 $\bar{1}$ 0] RHEED pattern, because the ordering and crystallinity of RuO₂ on Ru(0001) electrode are worse.

RL spacing of the hkl spots are determined by the following equation,

$$b_{hkl}^2 = \frac{h^2 + k^2}{a^2} + \frac{l^2}{c^2}, \text{ with } a = b = 4.49 \text{ \AA} \text{ and } c = 3.11 \text{ \AA}.$$

Furthermore, the relative intensities of the 101, 202, 301, 002 and 200 reflection spots in Figure 7A are examined and in qualitative agreement with the structure factors obtained by kinematic calculations shown in Table 1 [26]. With the structure factors (Table 1) we are also able to explain the systematic absence of particular reflection spots in the RHEED patterns (seen in Figure 5 and 6) [26], e.g., the structure factors of the (100), (010), (001), and (102) reflections are zero and these spots are also not observed in the RHEED patterns seen in Figure 5 and 6.

For comparison the [1 0 $\bar{1}$ 0] azimuths RHEED patterns for the Ru(0001) electrodes toward electrooxidation at +1.12 and +1.98 V are reversed as shown in Figure 6, for that the reflection spots 101, 121 and 200 depicted in Figure 6C can be clearly identified. The streaky reflections of the Ru substrate are still discernable in Figure 6A, proving parts of Ru(0001) electrode surface remain flat after electrooxidation at +1.12 V. While these Ru-streaky reflections are no longer visible in Figure 6B obtained at +1.98 V, proving the Ru electrode becomes completely rough. The extra (200)-spot develops at the (00)-rod in the RHEED pattern in Figure 5 and 6, showing that the RuO₂ clusters are indeed (100) oriented on Ru(0001) whose RL vector \underline{b}_{200} with magnitude, 0.445 Å⁻¹ is perpendicular to the substrate surface which gives the

Ru-oxide (100) layer spacing of $\frac{1}{2} a$. The estimated lattice constant a of the Ru-oxide is 4.5 Å in agreement with that of bulk RuO₂. The RuO₂ cluster is (100) oriented on Ru(0001) substrate aligned the [001] direction perpendicular to the $[1\ 0\ \bar{1}0]$ direction of Ru(0001). On the other hand, the (110) reflection spot ($0.314\ \text{\AA}^{-1}$) characteristic for the (110) oriented clusters does not appear along the (00)-rod in Figure 5 and 6C, proving the RuO₂ clusters are not (110) oriented on Ru(0001). The another lattice constant c perpendicular to a , parallel to the shadow edge of the RHEED pattern, is deduced from the distance ratio b_{11}/b_{002} , where b_{11} and b_{002} are the RL spacing of Ru(11) rod and the extra spot besides the (11) rod with respect to the (00) beam, respectively seen Figure 6C. The length of the reciprocal lattice vector \bar{b}_{200} of RuO₂ is $0.644\ \text{\AA}^{-1}$ giving $c = 3.11\ \text{\AA}$, e.g., the c vector of the Ru-oxide is parallel to the Ru(0001) substrate surface. It exhibits that the [001] Ru-atomic row spacing of the (100) RuO₂ clusters is 14% larger than that of the $[1\ 0\ \bar{1}0]$ of Ru(0001) substrate, proving the (100) RuO₂ clusters are incommensurately growing on Ru(0001). It is concluded, tentatively that the observed ruthenium oxide grown on Ru(0001) has a rutile structure exhibiting a tetragonal symmetry ($a_o = b_o = 4.50$, $c_o = 3.11\ \text{\AA}$) [26, 27].

As mentioned before the LEED pattern for the Ru(0001) electrode toward electrooxidation at +1.12 V reveals a (1 x 1) phase, where only the integral order spots appear, while the oxide reflection spots are invisible (as seen in Figure 5A). It implies that the structure and the epitaxial growth of RuO₂ clusters on Ru(0001) cannot be deduced by the LEED pattern analysis. In contrast, the extra spots of RuO₂ clusters developed in the RHEED pattern (Figure 5B and 6) allow us to determine the crystal structure of RuO₂ and the lateral orientation of the RuO₂ domains grown on Ru(0001) as explored in the following. Usually the LEED/RHEED patterns are the superimposed diffraction patterns of different domains. Therefore, we have to sort the reciprocal lattice nets of different oxide domains in the RHEED pattern, i.e., one has to classify the reflection spots in the RHEED pattern that belong to a certain reciprocal lattice net corresponding to a $[uvw]$ zone-axis pattern. For instance, the reflection spots connected by the red lines in the $[1\ 0\ \bar{1}0]$ azimuth RHEED pattern in Figure 7A are belonging to the relps of the (012)* reciprocal lattice net which is the [012] zone-axis pattern of RuO₂ domain II. The [012] zone-axis pattern is schematically represented in Figure 7B which is resulted from intersection of the reciprocal lattice of Ru-oxide with a reflection sphere at the zone axis $[uvw] = [012]$. Furthermore, it is found that the $[1\ 0\ \bar{1}0]$ azimuth RHEED pattern of Figure 7A is the superposition of the (010)* and (012)* reciprocal lattice nets, proving two rotational Ru-oxide domains are present on Ru(0001). The joined angle between the two zone-axis is around 60° as demonstrated in Figure 8, that allows the determination of the lateral orientation of the Ru-oxide domains I and II as exhibited in Figure 9A, in which the joined angle between the [001] axis of (100) Ru-oxide domain I and that of domain II is

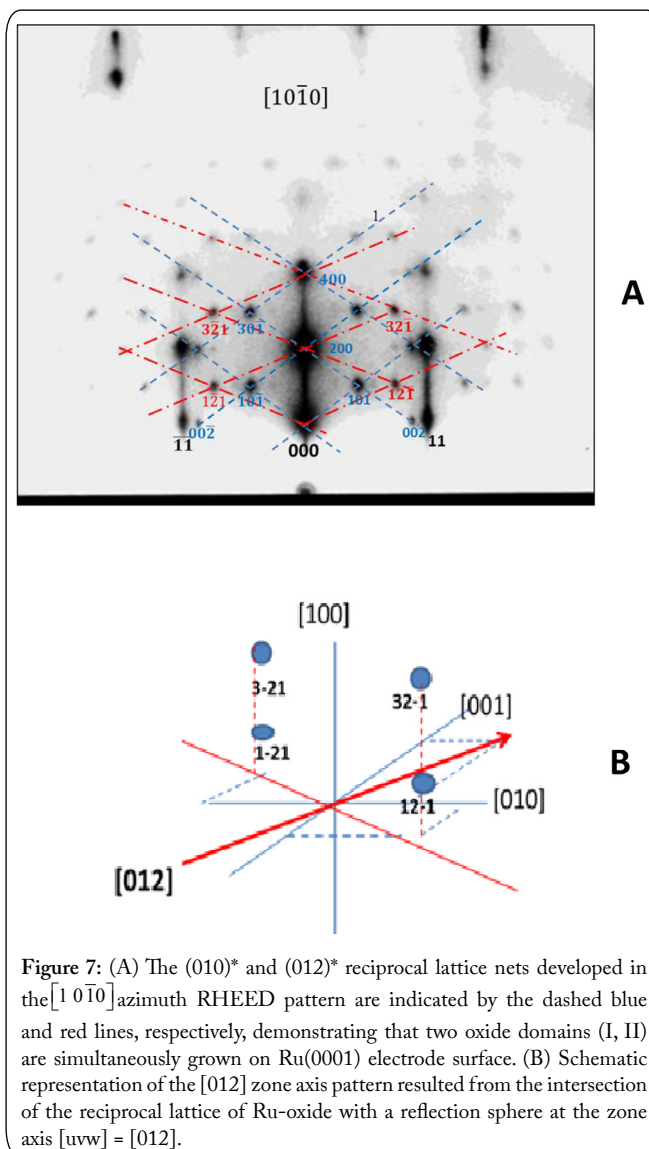


Figure 7: (A) The (010)* and (012)* reciprocal lattice nets developed in the $[1\ 0\ \bar{1}0]$ azimuth RHEED pattern are indicated by the dashed blue and red lines, respectively, demonstrating that two oxide domains (I, II) are simultaneously grown on Ru(0001) electrode surface. (B) Schematic representation of the [012] zone axis pattern resulted from the intersection of the reciprocal lattice of Ru-oxide with a reflection sphere at the zone axis $[uvw] = [012]$.

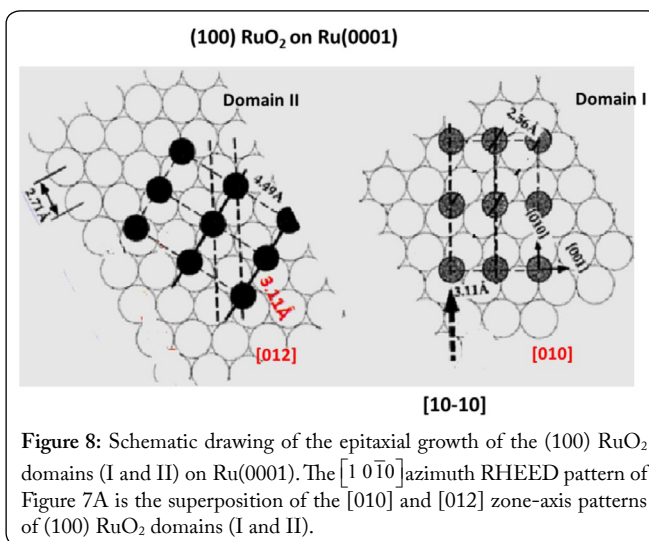
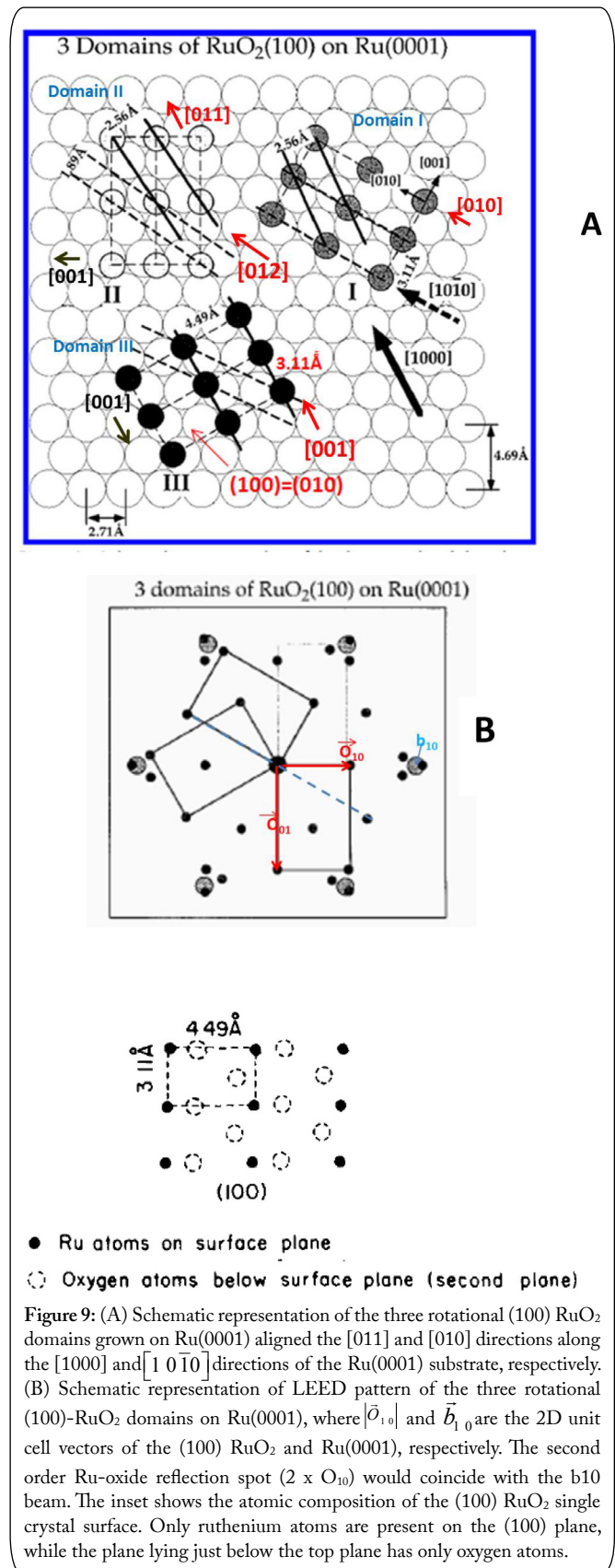


Figure 8: Schematic drawing of the epitaxial growth of the (100) RuO₂ domains (I and II) on Ru(0001). The $[1\ 0\ \bar{1}0]$ azimuth RHEED pattern of Figure 7A is the superposition of the [010] and [012] zone-axis patterns of (100) RuO₂ domains (I and II).

120°. In other words, the $[1\ 0\ \bar{1}0]$ azimuth RHEED pattern of Figure 5C is a diffraction pattern taken with an incident

electron beam along the $[1\ 0\ \bar{1}0]$ direction parallel to $[010]$ and $[012]$ lattice directions of the (100) RuO_2 domains I and II, respectively as shown in Figure 8.

It is shown that detailed analysis of the RHEED patterns allows us to determine the epitaxial growth and lateral orientation of the (100) RuO_2 domains (I and II) grown on Ru(0001) as illustrated in Figure 8. Although the extra spots of Ru-oxide domain (III) are invisible in the RHEED patterns in Figure 5C and 7A, the associated spots, 111, 222, 011 and 211 are detected in the $[1000]$ azimuth RHEED pattern obtained by 30° azimuthal rotation with respect to $[1\ 0\ \bar{1}0]$ azimuth as exhibited in Figure 5D and 5E. Actually the RHEED experiment performed at the $[1000]$ azimuth the diffraction pattern of RuO_2 domain II would give the $[011]$ zone-axis pattern, however, for convenient indexing we ascribe the above reflection spots to the $[0-11]$ zone axis pattern, e.g. 111, 222 instead of 1-11 and 2-22 spots, since the $[0-11]$ zone axis pattern is equivalent to the $[011]$ zone axis pattern, i.e., the extra spots in Figure 5E can be assigned to an RL $(0-11)^*$ or an $(011)^*$ net. For clarity, the extra spots belonging to the relps of the $(0\bar{1}1)^*$ RL net are connected by the red lines in Figure 5D, proving the $[1000]$ azimuth RHEED pattern is the superposition of the $(001)^*$ and $(0\bar{1}1)^*$ RL nets. It is worthy of mention that the $[011]$ zone-axis pattern is the diffraction pattern obtained by the electron incident direction along the $[011]$ direction of the Ru-oxide domain II parallel to $[1000]$ direction of Ru(0001) (referred to Figure 9A), while the diffraction pattern of the same Ru-oxide domain II at the $[1\ 0\ \bar{1}0]$ azimuth gives the $[012]$ zone-axis pattern which appears in the $[1\ 0\ \bar{1}0]$ azimuth RHEED pattern in Figure 7A. In order to become clear the $(0\bar{1}1)^*$ and $(001)^*$ RL nets observed in the $[1000]$ azimuth RHEED pattern (Figure 5C) are separately sketched in Figure 5E, where the $(0\bar{1}1)^*$ reciprocal lattice net is due to the (100) RuO_2 domain II, and the $(001)^*$ RL net is the $[001]$ zone axis pattern of the RuO_2 (100) domain III aligning the $[1000]$ direction of Ru(0001) (referred to Figure 9A). That is, all three of I, II and III (100) RuO_2 -domains are rotated by 120° with each other on Ru(0001) surface as illustrated in Figure 9A, in which the joined angles between the vector \vec{c} $[001]$ of the (100) RuO_2 domains I, II and III are 120° , respectively. The $[001]$ direction of RuO_2 domain III is parallel to $[1000]$ of Ru(0001). If the (100) Ru-oxide grows in a 2D well-ordered films on Ru(0001) as shown by Figure 9A, one would expect to see a LEED pattern containing the reflection spots of three rotational (100) RuO_2 domains as exhibited in Figure 9B. The unit cell vectors of the (100) RuO_2 crystal plane are depicted by \vec{O}_{10} and \vec{O}_{01} shown in Figure 9B, while b_{10} is the unit cell vector of the Ru substrate, i.e., $|\vec{O}_{10}| = 1/4.49$ and $|\vec{O}_{01}| = 1/3.11\text{\AA}$ are the reciprocal values of the $[100]$ and $[001]$ Ru-atomic row spacing of the (100) RuO_2 plane, respectively. It exhibits that the (100) RuO_2 clusters grow incommensurately on Ru(0001), where the (001) atomic row spacing of RuO_2 is 3.11\AA larger than that of the $[1\ 0\ \bar{1}0]$ row spacing of Ru substrate (2.71\AA) Furthermore the second order Ru-oxide



reflection $(2 \times \vec{O}_{10})$ would overlap with the Ru substrate beam b_{10} as shown in Figure 9B, so that both oxide- and the (10) Ru-reflections cannot be resolved in the RHEED pattern as seen in Figure 5D. The inset in Figure 9 shows the atomic composition of the (100) RuO_2 single crystal, where only

ruthenium atoms are present on the (100) plane, and the plane lying just below the top plane has only oxygen atoms. While both ruthenium and oxygen atoms are present on the (110) and (001) planes [27].

The missing oxide-spots in the LEED pattern for the (100) RuO₂ clusters on Ru(0001) is attributed to the fact that the nano-sized (~ 16 nm) RuO₂ crystallites are not pseudomorphic growth on Ru(0001) and strongly distorted. Few (100) Ru surface atoms of the nano-clusters are not perfectly scattered in phase and contribute too weak scattering intensity to “light up” the LEED reflection spots in line with that previously observed for Ru(0001) electrooxidation at +1.11 V for 2 min in 0.1 M HClO₄, for that LEED also shows a (1 x 1) [24]. An analogous result has been demonstrated by the Pd UPD onto Au(100), where a monolayer Pd shows a c (2 x 2) LEED pattern shown in Figure 10A, however, after partial dissolution of bulk Pd the roughened Pd layers on Au(100) give a (1 x 1) LEED pattern as seen Figure 10B [28]. In contrast, even for 1/4 ML coverage of the underpotentially deposited Cu on Au(111) shows an ordered ($\sqrt{3} \times \sqrt{3}$)R30° pattern both in LEED and RHEED referred to Figure 11 [29], in which the submonolayer Cu is a commensurate growth and very well ordered grown on Au(111) substrate giving rise to the $\sqrt{3}$ -reflections in the sub-Laue zones in the RHEED pattern in Figure 11, accordingly resulting in $\sqrt{3}$ LEED pattern. For the case of RuO₂ on Ru(0001), the whole oxide-clusters, e.g., ≈11 (100)-atomic oxide-layers contribute to RHEED reflection via a transmission electron diffraction, giving rise to bulk oxide reflections, where the RHEED reflections suffered only from

small momentum transfer perpendicular to the Ru-oxide surface so that the sensitivity to surface roughness of oxide and its crystal disorder is less severe than that with LEED. Consequently, the oxide reflections can still be detected in the zero-Laue zone as seen in Figure 6A and B. On the other hand, for LEED the momentum transfer perpendicular to the oxide surface is large, thus preventing LEED observation. Even tried various incident LEED electron energy the oxide spots could not be detected, since the higher order reflection of the oxide become considerably weak due to the crystal distortions of the (100) Ru-oxide referred to the RHEED pattern of Figure 6B and C.

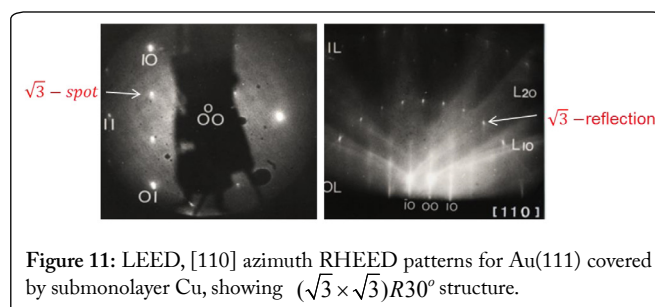


Figure 11: LEED, [110] azimuth RHEED patterns for Au(111) covered by submonolayer Cu, showing ($\sqrt{3} \times \sqrt{3}$)R30° structure.

In the following we compare the topology and crystallinity of the (100) RuO₂ clusters produced by electrooxidation on Ru(0001) with that obtained by alternative procedures reported in the literatures; Let us first compare the crystallinity of the (100) RuO₂ clusters on Ru(0001) generated at different oxidation potentials, e.g., at +1.12 and +1.98 V. The LEED pattern (Figure 5A) for the Ru(0001) electrode towards electro-oxidation at +1.12 V shows a (1 x 1) phase, while the 3D-spots of RuO₂ as well as Ru substrate reflections are observed by RHEED (Figure 5B) for the same sample, exhibiting that 3D-RuO₂ clusters rather than 2D RuO₂ films are formed on Ru(0001). The behavior of the Ru electrode may be ascribed as a continuous transition from hydroxyl adsorption to bulk hydroxide formation; $\text{Ru} + \text{OH}_{\text{ad}}^- \rightarrow \text{RuOH} + \text{e}^-$. It appears that the bonding energies between the Ru atoms and OH⁻ ions are strong relative to the bond between Ru^{x+} and Ru(0001) electrode at potential + 1.12 V which facilitates formation of bulk hydroxide RuOH and nucleation of 3D RuO₂ on Ru(0001) in the electrolyte solution. Although the observed oxide reflection spots are diffuse and broad as seen in Figure 5B and 6A, the higher order reflection spots 202 and 002 of RuO₂ are still discernable besides the Ru(11) reflection. However, these spots are no longer visible in the RHEED pattern for Ru-oxide produced at +1.98 V as seen in Figure 6C, where the oxide-spots become even broader than that of Figure 6A, suggesting that the RuO₂ clusters are smaller and their crystallinity even worse than that obtained at +1.12 V. In addition, the whole Ru electrode becomes completely rough confirmed by the appearance of the 3D Ru bulk spots in the RHEED patterns (Figure 6B), thereby the Ru electrode is evidently stronger attacked by OH⁻_{ad} species at more positive potential +1.98 V, enhancing the Ru atoms segregation, hydroxide formation and surface roughening. The reason for the 3D growth of RuO₂ clusters on Ru(0001) electrode is attributed to the fact that electrooxidation in acidic solution takes place via OH⁻ anion adsorption on the

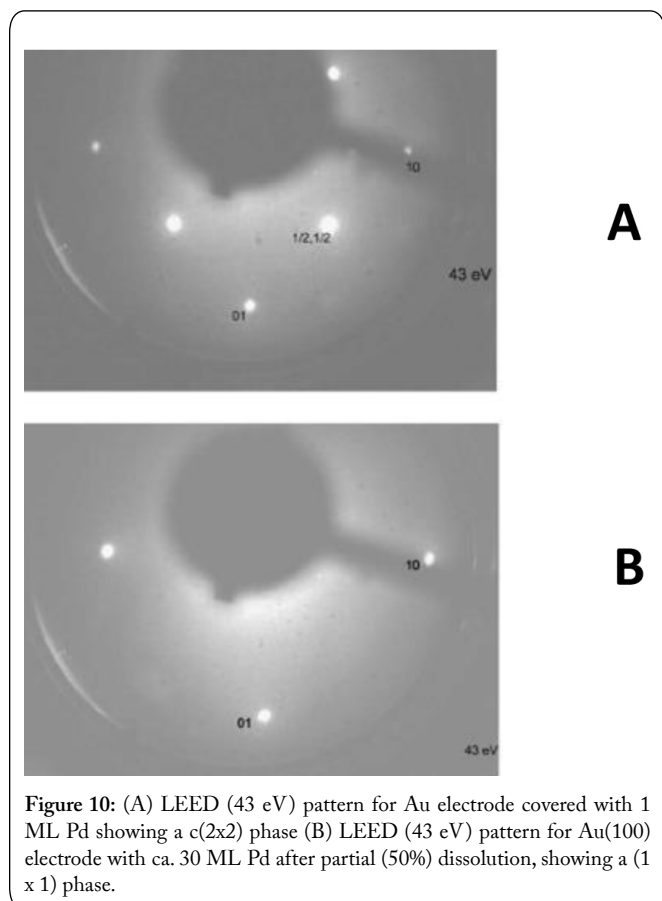


Figure 10: (A) LEED (43 eV) pattern for Au electrode covered with 1 ML Pd showing a c(2x2) phase (B) LEED (43 eV) pattern for Au(100) electrode with ca. 30 ML Pd after partial (50%) dissolution, showing a (1 x 1) phase.

Ru electrode as seen a pronounced anodic peak in CV curve in Figure 4, where a place exchange occurs between O/OH⁻ and the surface Ru-atoms, causing surface roughening of the Ru electrode [30, 31] giving rise to the Ru-transmission spots in the RHEED patterns (seen in Figure 5 and 6). It is in analogy to the facets formation on Pt(100) electrode after potential sweeping up to + 1.1 V in 0.01 M HClO₄ [32]. Contrary to the 3D RuO₂ cluster formation on Ru(0001) electrode, the gas phase oxidation at 700 K under UHV conditions tends to form chemisorbed O-islands on Ru(0001) [25], it induces the segregation of Ru-atoms to the surface. The Ru-atoms react in turn with the adsorbed oxygen at elevated temperatures forming patchy RuO₂ islands on Ru(0001) which assembles Al₂O₃ thin film growth on NiAl(100) [33, 34] where the strongly bonded O-species assist Al atoms segregation from NiAl(100) substrate. The free Al atoms turn to react with O_{ad} to Al₂O₃ on NiAl(100). As time progresses more RuO₂ islands are nucleated and then islands grow, coalesce and finally a smooth film ($\approx 20 \mu\text{m}$) is formed which then thickens ($\approx 1\text{-}2 \text{ nm}$) as has been determined by STM measurements [16]. Thus the topology and crystal ordering of the (100) RuO₂ clusters on Ru(0001) electrode are very different from the (110) RuO₂ film by gas phase oxidation on Ru(0001) at 700 K under UHV conditions; the latter grows layer by layer with a (110) orientation on Ru(0001) exhibiting a 2D well-ordered RuO₂ film as shown by a LEED pattern in Figure 12A [25]. A schematic drawing of the epitaxial growth of the (110) Ru-oxide-domains on Ru(0001) deduced by LEED pattern is illustrated in Figure 12B [25, 27]. The inset in Figure 12 shows the atomic composition of the (110) plane of RuO₂ where both Ru and O atoms are present, while only Ru atoms are present in the (100) RuO₂ plane [27]. The mechanism for the different orientation growth of (hkl) RuO₂ in liquid and gas phases is not yet clear.

Although the difference in lattice strain between the (100) RuO₂ and (110) RuO₂ on Ru(0001) is quite small [25], the observation of the (200) reflection spot of RuO₂ clusters in RHEED patterns in Figure 5, proving the RuO₂ clusters are oriented (100) on Ru(0001) electrode. A single crystal of (100) RuO₂ has also been prepared by a multizone furnace using a vapor transport method under oxygen flow [12]. It appears that (100) RuO₂ cluster reveals a lowest interface energy on Ru(0001) substrate [35], despite the relative large lattice misfit of around 10%. It is in analogy to RuO₂ growth on Ru(0001) substrate prepared at temperature 530 °C by in-situ sputtering [35], where RuO₂ film exhibits mixed (110) and (100) orientations, but the (100)-orientation is dominant, revealing that RuO₂ grows also in favor of (100) orientation on Ru(0001) in the gas phase conditions [35]. However, a well-ordered (110) RuO₂ film on Ru(0001) has been obtained by gas phase oxidation at a sample temperature of 700 K under UHV conditions [36]. The same RuO₂ film (110) oriented on MgO(100) has been observed by metal-organic vapor deposition at deposition temperature of 350 °C [37], while RuO₂ film (100) oriented on LaAlO₃ has been prepared at deposition temperature of 600 °C [38]. Similar results have also been observed for RuO₂ growth on glass or sapphire by reactive sputtering [39, 40]. Although both Pt(111) and Ru(0001) surfaces reveal an hexagonal structure, RuO₂ grows

with (100) on the former and with a (110) or a mixture of (100) and (110) orientations on the latter surface [35]. Good (111) orientation of the Pt substrate is a prerequisite for a (100)-RuO₂ growth. Furthermore, the RuO₂ prepared by electro-deposition on TiO₂ exhibited a crystalline phase characterized by XRD measurements [17]. While an amorphous RuO₂ has been obtained by cyclic deposition on titanium substrate, no diffraction peaks of RuO₂ were observed in the XRD pattern [18]. The PbZr_xTi_{1-x}O₃ (PZT) films were essentially randomly oriented on the randomly deposited RuO₂ on TiO₂ [41, 42], demonstrating that the orientation of PZT is very much influenced by the crystallinity of the RuO₂/TiO₂ substrate on which nucleation takes place. The “as-prepared” RuO₂ catalysts by a colloidal procedure deposited onto a Nafion 115 membrane showed no oxide diffraction peaks in the XRD pattern, while after calcination above 200 °C the XRD peaks developed that were assigned to RuO₂ in a tetragonal rutile structure [43]. Well-aligned RuO₂ thin film on yttria-stabilized zirconia (YSZ) buffered Si has been prepared at a temperature range 400-700 °C, but the films tend to be polycrystalline if the deposition is done at a substrate temperature outside of this range [44]. It reveals that the crystallinity of RuO₂ clusters/films is strongly influenced by substrate temperature; increasing the substrate temperature enhances the mobility of the deposited atoms and the ordering of RuO₂ clusters/films.

Based on the above results we may conclude that nucleation processes and epitaxial growth of RuO₂ clusters/films occurring in the different preparation methods are certainly very different in detail, however, the crystallinity of RuO₂ thin film is highly dependent on the substrate temperature and the substrate qualities on which the epitaxy takes place. Though the theory of lattice matching and interface energy is not well developed to allow its use in predicting epitaxial orientations, the nuclei orientation is strongly dependent on the growth environments, including reactant partial pressure, temperature, interfacial energies and gas/liquid phases [45]. Surprisingly, the “as prepared” RuO₂ clusters on Ru(0001) electrode in the present work exhibits a crystalline phase

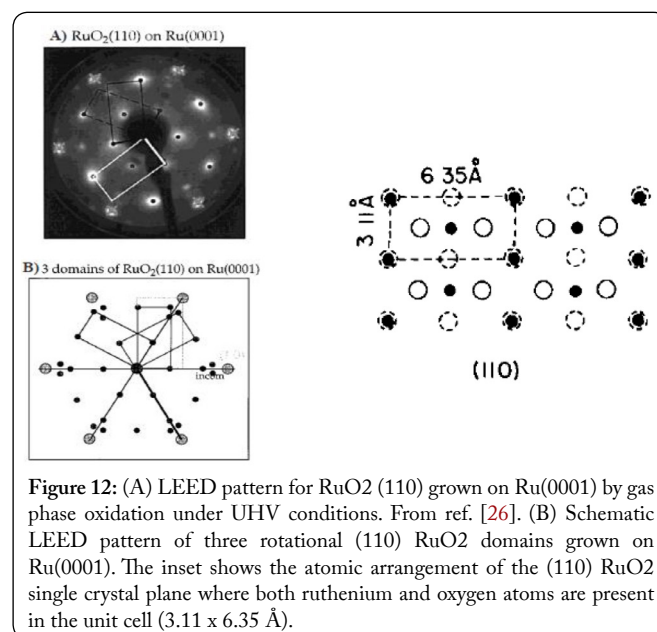


Figure 12: (A) LEED pattern for RuO₂ (110) grown on Ru(0001) by gas phase oxidation under UHV conditions. From ref. [26]. (B) Schematic LEED pattern of three rotational (110) RuO₂ domains grown on Ru(0001). The inset shows the atomic arrangement of the (110) RuO₂ single crystal plane where both ruthenium and oxygen atoms are present in the unit cell (3.11 x 6.35 Å).

without annealing, which is very different from that obtained by various procedures reported in the literatures. It should be emphasized that the structural characterization of the electrochemically prepared (100) RuO₂ on Ru(0001) could be achieved by RHEED pattern analysis, although the LEED shows only a (1 x 1) phase.

Conclusion

It is shown that the epitaxial growth of the RuO₂ cluster on Ru(0001) electrode formed by electro-oxidation could be reliably determined by RHEED; the RuO₂ cluster is exclusively (100) oriented on Ru(0001) and the $[1\ 0\ \bar{1}0]$ azimuth RHEED pattern analysis allows the determination of two (100) RuO₂ domains (I, II) rotated by 120° with each other grown on Ru(0001). The favored (100) orientation of RuO₂ clusters/films on Ru(0001) is likely due to its smaller interface free energy in the liquid phase. During the electro-oxidation the OH⁻ species are initially chemisorbed on Ru(0001) electrode at potential > 1.12 V causing the segregation of Ru atoms and bulk Ru-hydroxide formation. It then turns to cause roughening Ru-electrode surface and 3D RuO₂ clusters formation. The “as prepared” RuO₂ clusters on single crystal Ru(0001) electrode without calcination exhibit a mono-crystalline phase despite considerable crystallinity-disorders, which is very different from that obtained by other procedures. Considering the gas phase oxidation on Ru(0001) at 700 K under UHV conditions, the chemisorption of the O-species on Ru(0001) seems to serve as a precursor for the subsequent 2D-growth of (110) RuO₂ films on Ru(0001) analog to the Al₂O₃ thin films growth on NiAl(100).

References

- Morales-Ortiza U, Avila-Garciab A, Lara CVH. 2006. Ruthenium oxide films for selective coatings. *Sol Energy Mater Sol Cells* 90(6): 832-840. doi: 10.1016/j.solmat.2005.04.019
- Conway BE. 1999. Electrochemical Supercapacitors. Plenum Publishing, New York, USA.
- Kotz R, Carlen M. 2000. Principles and applications of electrochemical capacitors. *Electrochim Acta* 45(15-16): 2483-2498. doi: 10.1016/S0013-4686(00)00354-6
- Sarangapani S, Tilak BV, Chen CP. 1996. Materials for electrochemical capacitors. Theoretical and experimental constrains. *J Electrochem Soc* 143(11): 3791-3799. doi: 10.1149/1.1837291
- Ashcroft AT, Cheetham AK, Foord JS, Green MLH, Grey CP, et al. 1990. Selective oxidation of methane to synthesis gas using transition metal catalysts. *Nature* 344: 319-321. doi: 10.1038/344319a0
- Arriaga LG, Martinez W, Cano U, Blud H. 2007. Direct coupling of a solar-hydrogen system in Mexico. *Int J Hydrogen Energy* 32(13): 2247-2252. doi: 10.1016/j.ijhydene.2006.10.067
- Marshall A, Borresen B, Hagen G, Tsyppkin M, Tunold R. 2005. Preparation and characterization of nanocrystalline Ir_xSn_{1-x}O₂ electrocatalytic powders. *Mater Chem Phys* 94(2-3): 226-232. doi: 10.1016/j.matchemphys.2005.04.039
- Da Silva LM, Boodts JFC, De Faria LA. 2001. Oxygen evolution at RuO₂(x)+Co₃O₄(1-x) electrodes from acid solution. *Electrochim Acta* 46(9): 1369-1375. doi: 10.1016/S0013-4686(00)00716-7
- Cornell A, Simonsson D. 1993. Ruthenium Dioxide as cathode material for hydrogen evolution in hydroxide and chlorate solutions. *J Electrochem Soc* 140(11): 3123-3129. doi: 10.1149/1.2220996
- Tamura H, Iwakura C. 1982. Metal oxide anodes for oxygen evolution. *Int J Hydrogen Energy* 7(11): 857-863. doi: 10.1016/0360-3199(82)90003-9
- Oppedisano DK, Jones LA, Junk T, Bhargava SK. 2014. Ruthenium electrodeposition from aqueous solution at high cathodic overpotential. *J Electrochem Society* 161(10): D489-D494. doi: 10.1149/2.0441410jes
- Hadzi-Jordanov S, Angerstein-Kozłowska H, Vukovic M, Conway BE. 1978. Reversibility and growth behavior of surface oxide films on ruthenium electrodes. *J Electrochem Soc* 125(9): 1471-1480. doi: 10.1149/1.2131698
- Lister TE, Chu Y, You H, Nagy Z. 1999. Reduction of the Ruthenium Dioxide (100) surface: origin of ultracapacitance. Materials Science Division, Argonne National Laboratory, Argonne, IL, USA.
- Kim YD, Schwegmann S, Seitsonen AP, Over H. Epitaxial growth of RuO₂(100) on Ru(1010): Surface structure and other properties. *J Phys Chem B* 105(11): 2205-2211. doi: 10.1021/jp003650y
- Böttcher A, Rogozia M, Niehus H, Over H, Ertl G. 1999. Transient experiments on CO₂ formation by the CO oxidation reaction over oxygen-rich Ru(0001) surfaces. *J Phys Chem* 103(30): 6267-6271. doi: 10.1021/jp990503v
- Over H, Kim YD, Seitsonen AP, Wendt S, Lundgren E, et al. 2000. Atomic-scale structure and catalytic reactivity of the RuO₂(110) surface. *Science* 287(5457): 1474-1476. doi: 10.1126/science.287.5457.1474
- Gujar TP, Kim WY, Puspitasari I, Jung KD, Joo OS. 2007. Electrochemically deposited nanograin Ruthenium oxide as a pseudocapacitive electrode. *Int J Electrochem Sci* 2: 666-673.
- Hu CC, Huang YH. 1999. Cyclic voltammetric deposition of Hydrous Ruthenium oxide for electrochemical capacitors. *J Electrochem Soc* 146(7): 2465-2471. doi: 10.1149/1.1391956
- Zei MS. 2015. Epitaxial growth of Co and Ru on Pt(111). *J Phys Chem C* 119(6): 3091-3101. doi: 10.1021/jp5104559
- Lehmpfuhl G, Uchida Y, Zei MS, Kolb DM. 1999. Electron diffraction and electron microscopy of electrode surfaces. In: Lipkowski J, Ross PN (eds) Imaging of surfaces and interfaces: Frontiers of electrochemistry. Wiley-VCH: Weinheim, Germany, pp 57.
- Wu K, Zei MS. 1998. Electrochemical behavior and structural changes of a reconstructed Pt(100) electrode in sulfuric acid: a comparison with Pt(100)-(1x1). *Surf Sci* 415(1-2): 212-226. doi: 10.1016/S0039-6028(98)00597-4
- Zei MS, Lei T, Ertl G. 2003. Spontaneous and electrodeposition of Pt on Ru(0001). *Zeitschrift für Phys Chem* 217(5): 447-457. doi: 10.1524/zpch.217.5.447.20460
- Kolb DM, Lehmpfuhl G, Zei MS. 1990. Surface structural investigations by electron diffraction techniques. In: Gutierrez C, Melendres C (eds) Spectroscopic and diffraction techniques in interfacial electrochemistry. Springer Netherlands, Netherlands, pp 361-382. doi: 10.1007/978-94-011-3782-9_12
- Lin WF, Zei MS, Eiswirth M, Ertl G, Iwasita T, et al. 1999. Electrocatalytic activity of Ru-modified Pt(111) electrode toward CO oxidation. *J Phys Chem B* 103(33): 6968-6977. doi: 10.1021/jp9910901
- Lin WF, Zei MS, Kim YD, Over H, Ertl G. 2000. Electrochemical versus gas-phase oxidation of Ru single crystal surfaces. *J Phys Chem B* 104: 6040-6048. doi: 10.1021/jp0003149
- Vogel W. 1999. Private communication.
- O'Grady WE, Atanasoska L, Pollak FH, Park HL. 1984. Single crystal RuO₂ (110): surface structure. *J Electroanal Chem* 178(1): 61-68. doi: 10.1016/S0022-0728(84)80023-6
- Pinheiro ALN, Zei MS, Luo MF, Ertl G. 2006. The epitaxial growth of Pd electrodeposition on Au(100) studied by LEED and RHEED. *Surf Sci* 600(3): 641-650. doi: 10.1016/j.susc.2005.10.057
- Nakei Y, Zei MS, Kolb DM, Lehmpfuhl G. 1984. A LEED and RHEED investigation of Cu on Au(111) in the underpotential region. *Ber Bunsenges Phys Chem* 88(4): 340-345. doi: 10.1002/bbpc.19840880405

30. Schultze JW. 1980. Electrodes of Conductive Metallic Oxides, Part A, Trasatti S (Ed.). Elsevier, New York, USA. doi: 10.1002/bbpc.19810850527
31. Nichols J, Magnussen OM, Hotlos J, Twomey T, Behm RJ, et al. 1990. An *in-situ* STM study of potential-induced changes in the surface topography of Au(100) electrodes. *J Electroanal Chem* 290(1-2): 21-31. doi: 10.1016/0022-0728(90)87417-1
32. Zei MS, Ertl G. 1999. On the structural transformation of the reconstructed Pt(100) in electrolyte solutions. *Surf Sci* 442(1): 19-26. doi: 10.1016/S0039-6028(99)00806-7
33. Zei MS, Lin CS, Wen WH, Chiang CI, Luo MF. 2006. Growth of Al₂O₃ thin films on NiAl(100) by gas-phase oxidation and electro-oxidation. *Surf Sci* 600(9): 1942-1951. doi: 10.1016/j.susc.2006.02.036
34. Freund HJ, Kühlenbeck H, Staemmler V. 1996. Oxide surfaces. *Rep Progr Phys* 59(3): 283-347. doi: 10.1088/0034-4885/59/3/001
35. Maeder T, Murali P, Sagalowicz L. 1999. Growth of (111)-oriented PZT on RuO₂(100)/Pt(111) electrodes by *in-situ* sputtering. *Thin Solid Films* 345(2): 300-306. doi: 10.1016/S0040-6090(98)01420-5
36. Böttcher A, Niehus H, Schwegmann S, Over H, Ertl G. 1997. CO oxidation reaction over oxygen rich Ru(0001) surfaces. *J Phys Chem* 101(51): 11185-11191.
37. Gao Y, Bai G, Liang Y, Dunham GC, Chambers SA. 1997. Structure and surface morphology of highly conductive RuO₂ films grown on MgO by oxygen-plasma-assisted molecular beam epitaxy. *J Mater Res* 12(7): 1844-1849. doi: 10.1557/JMR.1997.0253
38. Lu P, He S, Li FX, Jia QX. 1999. Epitaxial growth of RuO₂ thin films by metal-organic chemical vapor deposition. *Thin Solid Films* 340(1-2): 140-144. doi: 10.1016/S0040-6090(98)01396-0
39. Kaga Y, Abe Y, Yanagisawa H, Sasaki K. 1998. Formation process and electrical property of RuO₂ thin films prepared by reactive sputtering. *Jpn J Appl Phys* 37(1): 3457. doi: 10.1143/JJAP.37.3457
40. Meng LJ, dos Santos MP. 1999. Characterization of RuO₂ films prepared by rf reactive magnetron sputtering. *Appl Surf Sci* 147(1-4): 94-100. doi: 10.1016/S0169-4332(99)00089-6
41. Zielkowski J. 1989. New method of calculation of the surface enthalpy of solids. *Surf Sci* 209(3): 536-561. doi: 10.1016/0039-6028(89)90095-2
42. Maeder T, Murali P, Sagalowicz L, Reaney I, Kohli M, et al. 1996. Pb(Zr, Ti)O₃ thin films on zirconium membranes for micromechanical applications. *Appl Phys Lett* 68(6): 776-779. doi: 10.1063/1.116529
43. Cruz JC, Baglio V, Siracusano S, Antonucci V, Arico AS, et al. 2011. Preparation and characterization of RuO₂ catalysts for oxygen evolution in a solid polymer electrolyte. *Int J Electrochem Sci* 6(12): 6607-6619.
44. Jia QX, Song SG, Wu XD, Cho JH, Foltyn SR, et al. 1996. Epitaxial growth of highly conductive RuO₂ thin films on (100) Si. *Appl Phys Lett* 68(8): 1069-1071. doi: 10.1063/1.115715
45. Ueda R, Mullin JB. 1975. Crystal growth and characterization. North Holland Publishing Company, Amsterdam, Netherlands.